nature electronics

Article

https://doi.org/10.1038/s41928-024-01151-x

A multifunctional display based on photo-responsive perovskite light-emitting diodes

Received: 21 June 2022

Accepted: 14 March 2024

Published online: 10 April 2024

Check for updates

Chunxiong Bao[1,2,7], Zhongcheng Yuan[1,3,7], Wenxiao Niu[2], Jie Yang[4], Zijian Wang[2], Tao Yu[2], Jianpu Wang[4,5] & Feng Gao[1,6]

Current display screens are typically only used for information display, but can have a range of different sensors integrated into them for functions such as touch control, ambient light sensing and fingerprint sensing. Photo-responsive light-emitting diodes (LEDs), which can display information and respond to light excitation, could be used to develop future ultra-thin and large screen-to-body ratio screens. However, photo-response is difficult to achieve with conventional display technologies. Here, we report a multifunctional display that uses photo-responsive metal halide perovskite LEDs as pixels. The perovskite LED display can be simultaneously used as a touch screen, ambient light sensor and image sensor (including for fingerprint drawing) without integrating any additional sensors. The light-to-electricity conversion efficiency of the pixels also allow the display to act as a photovoltaic device that can charge the equipment.

Display screens are an essential component of many modern electronic devices, including smart phones, smart watches, laptops and tablets. Conventional displays—including liquid crystal displays and organic light-emitting diode (LED) displays—can only perform a single function of information display. Therefore, additional sensors have to be integrated into displays for functions such as touch control, ambient light sensing and fingerprint sensing (Fig. 1a). However, these additional sensors increase cost and complexity, limiting the development of ultra-thin and large screen-to-body ratio screens.

A promising strategy to advance display technology is to develop photo-responsive LEDs, which could be used to incorporate the functions of different sensors into the pixels of a display. However, this is challenging for market-dominating display techniques (such as liquid crystal and organic LED displays) due to the absence and/or weakness of sensing function in the display pixels[1,2]. LEDs based on cadmium selenide nanocrystals can offer photosensitivity, but their weak photo-response, which results from the intrinsic trade-off between light absorption and charge transport in nanocrystals, limits their development and application potential[3].

Perovskite LEDs (PeLEDs) are promising emitters for high quality displays due to their high colour purity, high efficiency, high brightness, and compatibility with both solution and vacuum deposition processes[4–7]. In addition, they can exhibit high optical absorption and outstanding carrier transport, making them promising materials for the development of photo-responsive LEDs that could be used as pixels in multifunctional displays. For example, highly efficient perovskite solar cells have been shown to efficiently emit light on the application of forward bias[8–16], and highly efficient PeLEDs have been used to efficiently detect light[17]. However, these systems used perovskite devices in the near-infrared range as light emitters or detectors, which are not relevant for practical display applications.

[1]Department of Physics, Chemistry and Biology (IFM), Linköping University, Linköping, Sweden. [2]National Laboratory of Solid State Microstructures, School of Physics, Nanjing University, Nanjing, China. [3]Clarendon Laboratory, Department of Physics, University of Oxford, Oxford, UK. [4]Key Laboratory of Flexible Electronics, Institute of Advanced Materials and School of Flexible Electronics (Future Technologies), Nanjing Tech University (NanjingTech), Nanjing, China. [5]School of Materials Science and Engineering & School of Microelectronics and Control Engineering, Changzhou University, Changzhou, China. [6]Center of Artificial Photosynthesis for Solar Fuels and Department of Chemistry, School of Science, Westlake University, Hangzhou, China. [7]These authors contributed equally: Chunxiong Bao, Zhongcheng Yuan. e-mail: feng.gao@liu.se

https://doi.org/10.1038/s41928-024-01151-x

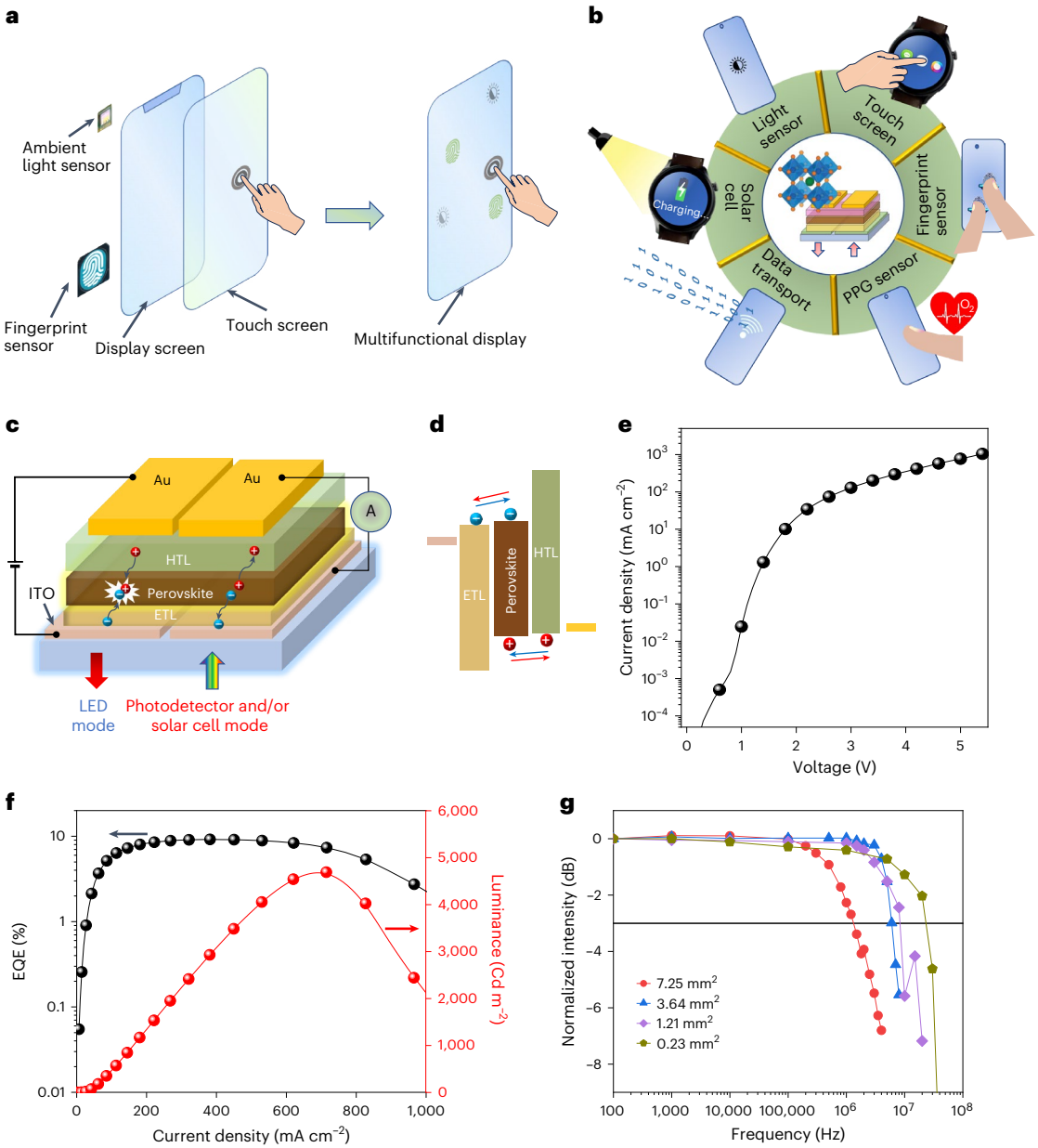

Fig. 1 | Concept of the multifunctional display, device structure and electroluminescence performance of photo-responsive PeLEDs. **a**, Illustration of conversional display screens integrated with additional functional sensors and the concept of the multifunctional display screen. **b**, Illustration of functions realized by the multifunctional display. **c**, Schematic structure of the photo-responsive PeLEDs. ETL, electron transport layer; HTL, hole transport layer. **d**, The energy level alignment of the photo-responsive PeLEDs. **e**, *J*–*V* curve of the red PeLED. **f**, EQE and *L*–*J* curves of the red PeLED. **g**, Frequency response of the PeLEDs with different device working areas.

In this Article, we report efficient PeLEDs that emit in the visible region and have excellent photoresponsivity. The combination of bright emission and high photo-response make PeLEDs promising candidates for the development of multifunctional displays (Fig. 1b). We use this approach to create a multifunctional display that can be used as a touch screen, ambient light sensor and image sensor (including fingerprint drawing, which indicates promise as a fingerprint sensor). We also show that display can be used for photoplethysmography (PPG), and that it can be used to covert ambient light into electricity and charge a supercapacitor.

Electroluminescence performance of photo-responsive PeLEDs

Light emission (for LEDs) and light absorption (for detectors and solar cells) are reciprocity processes. On charge injection under the forward bias in LEDs, electrons and holes recombine radiatively, generating light emission. On light excitation in detectors or solar cells, photogenerated carriers are separated under the built-in and/or external electrical field and then collected by electrodes. Due to the different working mechanisms of LEDs and detectors and/or solar cells, it is necessary to design suitable device structures and energy level alignment for realizing both functions in the same device (that is, photo-responsive PeLEDs shown in Fig. 1c,d). To make sure that the carriers can be effectively injected (or extracted) in the LED (or detector and/or solar cell) model, we optimize the charge transport layers, avoiding high energy barrier between the perovskite and charge transport layers (Fig. 1d). For example, for red emitting devices we use zinc oxide (ZnO) nanoparticles and poly(9,9-dioctylfluorene-co-*N*-(4-butylphenyl)diphenylamine) (TFB) as the electron and hole transport materials, respectively, both of which have been demonstrated as effective charge transport layers in high-performance perovskite solar cells and LEDs[18–20].

https://doi.org/10.1038/s41928-024-01151-x

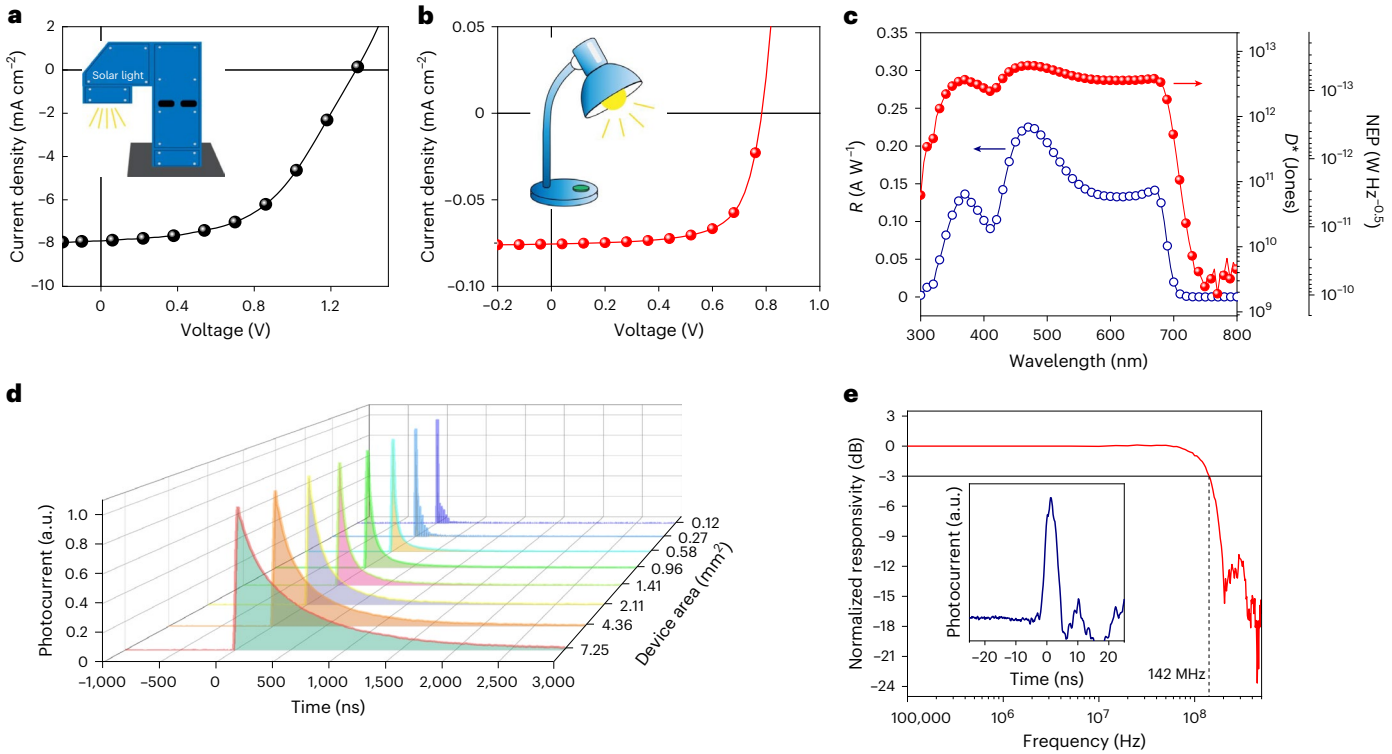

Fig. 2 | Photo-response performance and response speed of PeLEDs. a,**b**, *J*–*V* curves of our photo-responsive PeLED working as a photovoltaic device under illumination of an AM 1.5 G solar simulator (**a**) and a white LED (**b**) (4,000 K, 1,000 lux), respectively. **c**, Photoresponsivity (*R*), specific detectivity (*D**) and noise equivalent power (NEP) spectra of the PeLED working at the photodetector mode. **d**, TPC curves of perovskite diodes with different device working areas as photodetectors. **e**, Frequency response of the 0.06 mm^2 perovskite device working at the photodetector mode. The inset shows the TPC curve of the device.

Among different perovskite emitters, we choose three-dimensional (3D) perovskites as the active layers since low-dimensional perovskites (2D or perovskite quantum dots) possess high exciton binding energy, limiting efficient charge separation and hence the light-to-electricity conversion efficiency[21]. Accordingly, we use 3D $CsPbI_{3-x}Br_x$ as active layers for red multifunctional devices. The same as normal PeLEDs, additive engineering plays an important role for optimizing the performance of photo-responsive PeLEDs. We optimize the electroluminescent performance of the red PeLEDs by employing 5-ammonium valeric acid iodide (5-AVAI) as a processing additive in the $CsPbI_{3-x}Br_x$ emitters. The incorporation of 30% 5-AVAI helps to deliver an optimized external quantum efficiency (EQE) approaching 10% (Supplementary Fig. 1), where the electroluminescence intensity angular distribution follows a Lambertian profile (Supplementary Fig. 2). The device performance agrees well with the results of the photoluminescence quantum efficiency (PLQE) measurements, where the perovskite emitter processed with 30% 5-AVAI presents the highest PLQE (Supplementary Fig. 3), suggesting that using 5-AVAI in the perovskite emitters facilitates low defect densities, leading to improved LED performance.

On the basis of the current density–voltage (*J*–*V*) curve, EQE and luminance–current density (*L*–*J*) curves in Fig. 1e,f, a peak EQE of 9.7% (average value 8.41 ± 1.15%, Supplementary Fig. 4a) is obtained at a current density of roughly 400 mA cm^{-2}, along with luminance of 2,400 cd m^{-2} at this operating point. The device reaches a maximum luminance of roughly 4,700 cd m^{-2} at a high current density of roughly 715 mA cm^{-2}, where an EQE value of roughly 7.4% is maintained, demonstrating low efficiency roll-off. In addition, our device demonstrates decent stability, with an operational lifetime (T_{80}, duration of a device degrading to 80% of its initial brightness) of 18.5 hours at an initial luminance of around 100 cd m^{-2} (Supplementary Fig. 4b) and a stable electroluminescence peak position during the entire stability test (Supplementary Fig. 4c).

Switching speed is an important factor to consider when using PeLED pixels in displays. We show the frequency-dependent normalized electroluminescence intensities in Fig. 1g. The device with an active area of 7.25 mm^2 shows a −3 dB frequency up to 1.3 MHz, which is sufficient for low-speed data transmitting. The speed of our LED increases with decreasing device area, showing a −3 dB frequency of 22 MHz for the device with an area of 0.2 mm^2. Supplementary Fig. 5 shows waveforms of the electroluminescence signals of the device driven by a square-wave voltage with frequencies of 100 Hz and 22 MHz. The evident area-dependent speed of our devices indicates that the speed of our devices is mainly limited by the resistance–capacitance constant at present area ranges. A higher switching speed is expected by further reducing the device area, considering a much smaller area of pixels in practical normal-size displays (<5,000 μm^2).

Photo-response performance of photo-responsive PeLEDs

In addition to the potential application as light-emitting pixels for displays, our devices show remarkable photo-response as solar cells and photodetectors. The optimized red-emissive PeLEDs (incorporated with 30% 5-AVAI) show a power conversion efficiency of 5.34% under the air mass (AM) 1.5 G conditions and 12.6% under indoor light (white LED, 4,000 K, 1,000 lux), respectively (Fig. 2a,b), where the photovoltaic performance of devices based on perovskite layers with different additive amounts can be found in Supplementary Fig. 6. The higher efficiency under indoor light benefits from the good match between the response spectra of our devices and the emission spectrum of commercial white LEDs (Supplementary Fig. 7).

Excellent photo-response of the devices also indicates a potential optical sensing application of the devices. Due to the effective defect passivation of the perovskite layer, the optimized device shows a peak photoresponsivity of 0.23 A W^{-1} at 475 nm (Fig. 2c) and a remarkable

https://doi.org/10.1038/s41928-024-01151-x

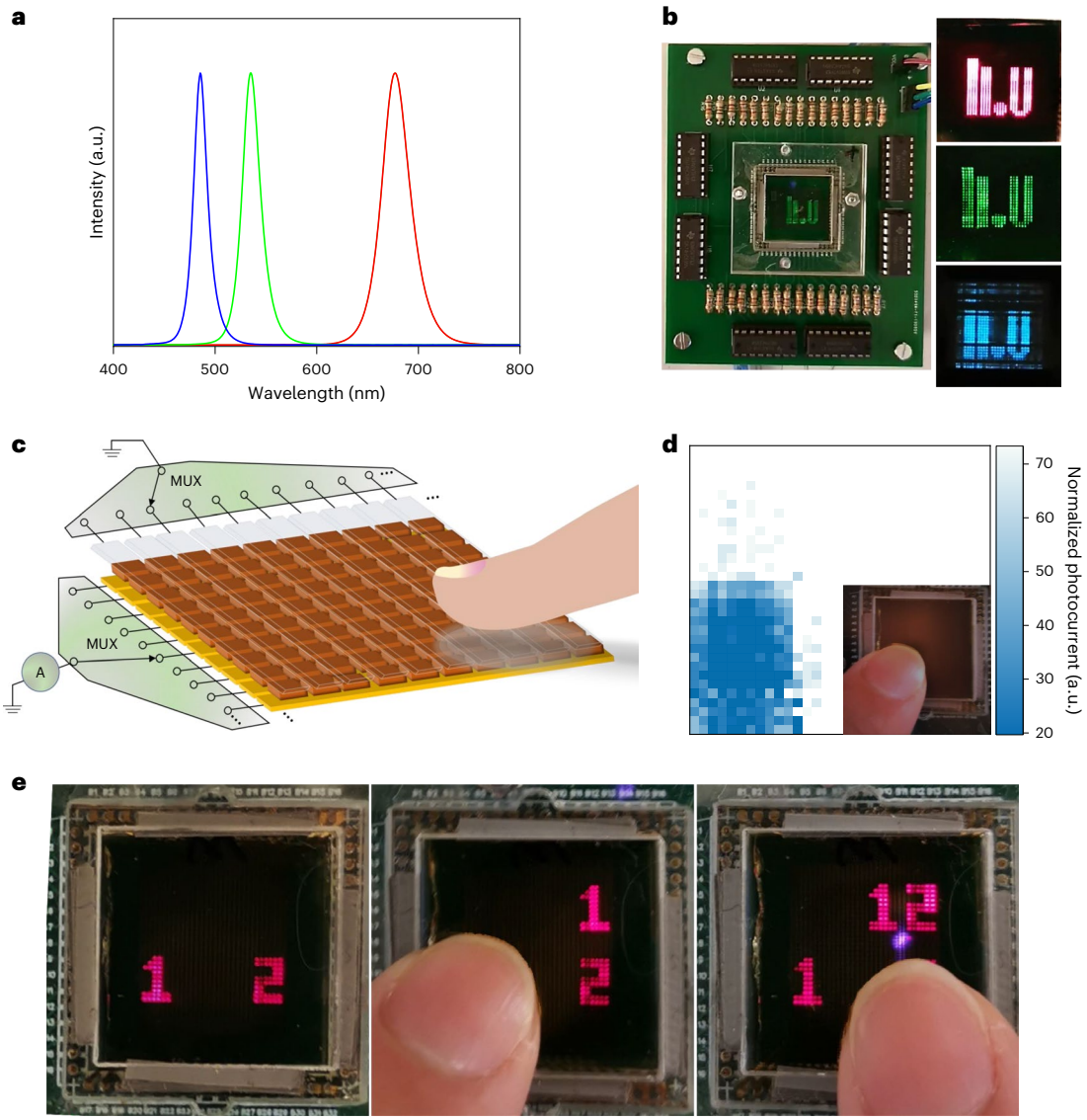

Fig. 3 | Display and touch control of PeLED display. a, Electroluminescence spectra of the photo-responsive PeLEDs emitting in red, green and blue region, respectively. **b**, Photographs of our proof-of-concept display demonstration system. The right three figures are displays prepared with red, green and blue PeLEDs. **c**, Schematic demonstration of the touch sensing function. MUX (multiplexer) is a data selector, realized by a switch array here. **d**, The photocurrent mapping result of the display after touch (the inset shows the real touch position on the display). **e**, Demonstration of 'inputting information function' through touching the multifunctional perovskite display screen. Here we input the characters 1 and 2, using the touch screen function of our display.

low dark current noise of roughly 10 fA $Hz^{-0.5}$ (Supplementary Fig. 8). Further calculations indicate that our PeLED shows a low noise equivalent power and high peak specific detectivity (D^*) of 44 fW $Hz^{-0.5}$ and 6.08×10^{12} Jones (Fig. 2c), respectively, which are among the most sensitive perovskite photodiodes (Supplementary Table 1)[22–28].

Response speed is one of the most important parameters for an optical signal detecting device. Figure 2d shows the transient photocurrent (TPC) curves of the devices with different device areas when working at the photodetector mode. We notice that the device working area has a direct impact on the response time, as widely reported in literature[17,24,26,29]. This suggests that the response speed of our devices operating in the photodetector mode is also constrained by the resistance–capacitance constant. For devices with an area above 0.12 mm^2, the response time is apparently determined by the falling time. By fitting the TPC curves with a single exponential function, we obtain a decreasing falling time from 520 ns for the 7.25 mm^2 area device to 7.5 ns for the 0.12 mm^2 area device (Supplementary Fig. 9). When the device area further decreases to 0.06 mm^2, the raising time is comparable to the falling time, and the TPC curve shows a pulse feature with a full-width at half-maximum of around 3.8 ns (inset in Fig. 2e). The response curve at the frequency domain (Fig. 2e) is obtained by performing the fast Fourier transform to the TPC curve. A −3 dB frequency of 142 MHz can be achieved with a 0.06 mm^2 device, indicating that our devices are among the fastest photodetectors based on solution-processed semiconductors (Supplementary Table 1)[28–31].

Proof-of-concept multifunctional displays

Encouraged by the excellent performance for light emission and detection, we now demonstrate the potential application of our devices in a multifunctional display using a proof-of-concept device. The 1,024 pixels proof-of-concept display (Supplementary Fig. 10), where the pixel area (0.2 × 0.3 mm^2) is defined by the overlap between the indium tin oxide (ITO) and Au electrodes, is fabricated following the same procedures as the PeLED demonstrated above. We can control the on and off state of every pixel using shift registers for information display. In addition to red PeLEDs, which are the focus of this work, we also

https://doi.org/10.1038/s41928-024-01151-x

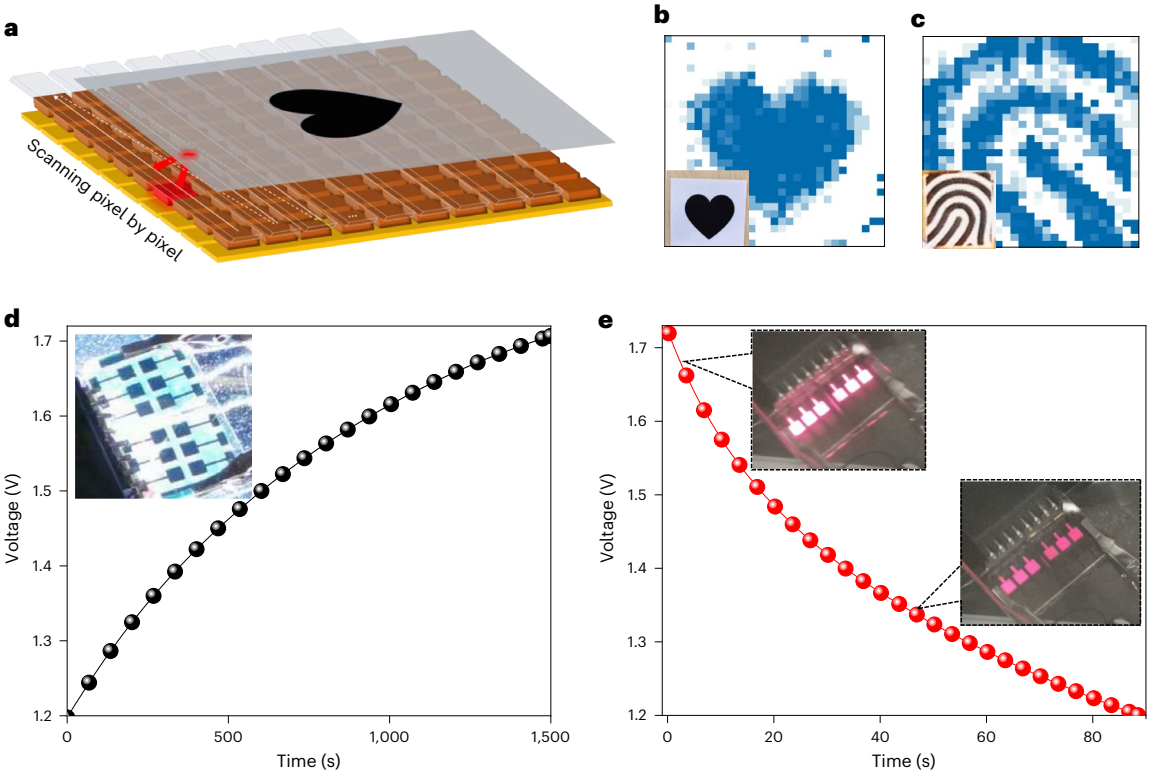

Fig. 4 | Advanced applications of PeLED display. a, Schematic process of surface imaging through optical scanning using the multifunctional perovskite display. **b**,**c**, Scanned images of a heart shape (**b**) and enlarged fingerprint drawing (**c**) (insets show the photographs of the original shapes), where the imaging area is 1.3 × 1.6 cm^2. **d**, The voltage-charging time curve of a supercapacitor when charged with our photo-responsive PeLED working at photovoltaic mode. Inset shows the image of the illuminated devices. **e**, Voltage attenuation curve of the charged supercapacitor when powering the same PeLEDs. During this process, the voltage of the supercapacitor decreases from ~1.7 to 1.2 V. Inset shows the images of the emissive PeLEDs working at different voltages.

fabricate green and blue PeLEDs using $FAPbBr_3$ and $CsPbBr_{3-x}Cl_x$ as emitters, respectively; both green and blue devices show bright emission and at the same time decent photo-response (Supplementary Fig. 11 and Supplementary Table 2). In Fig. 3a, we show the electroluminescence spectra of our red, green and blue emitting PeLEDs. Even though the colour rendition needs to be further improved for practical applications, simultaneous decent photo-response and bright emission indicate the potential of using PeLEDs in future photo-responsive full-colour displays. Digital photographs of our proof-of-concept devices displaying the logo of Linköping University (LiU) in red, green and blue colours are shown in Fig. 3b, with the corresponding video shown in the Supplementary Video. The demonstration indicates that our devices are sufficient in brightness and operation speed for a practical small-area passive-matrix display.

The touch screen function is realized by mapping the photocurrent response of the pixels on the touch action, where the light can be either from the external light (for example, room light) or from adjacent pixels that work under the LED mode (useful for applications in darkness). By scanning the photocurrent of each pixel and monitoring the photocurrent variations, we can locate the accurate touch position (Fig. 3c). We exemplify the touch function of our proof-of-concept display by covering the bottom left corner with a finger under the room light (inset shown in Fig. 3d). We detect much lower photocurrent from the pixels within the touch area as compared to those outside the touch area (Fig. 3d). Accordingly, with this practical proof-of-concept display, we can achieve accurate touch control for information input. Different information (here we use characters 1 and 2 as examples) can be input by touching different positions of the display (Fig. 3e and Supplementary Video).

We demonstrate that our photo-responsive perovskite display can also be used as a self-illuminated image sensor (Fig. 4a). The light emitted from the pixel working under the LED mode is reflected by the imaging object and then detected by another (neighbouring) pixel working under the photodetector mode, generating different photocurrent depending on the image of the object surface. As such, we can reproduce the surface image of the object by collecting the photocurrent of each pixel through pixel-by-pixel scanning (Fig. 4b). The imaging function of our display makes it promising for the application of screen-based scanner, where full-colour imaging can be readily realized based on a full-colour photo-responsive display.

Our multifunctional display also opens up new possibilities for on-screen multi-point fingerprint recognition. Fingerprint recognition is one of the most popular security and access control strategies in modern electronics. Traditionally, a fingerprint can only be input within a specific area of the screen where the fingerprint sensor is positioned. Multi-point fingerprint recognition solutions have now received increasing attention due to their attractive user experience, such as encryption, unlocking for different specific apps and joint signature with fingerprints. The photo-responsive PeLED display is promising for fingerprint sensing on the full area of the display. Since the resolution of our proof-of-concept display is not high enough for real fingerprint, we make use of enlarged fingerprint drawing printed on a piece of white paper with black ink (shown in the inset of Fig. 4c). A clear image (Fig. 4c) of the enlarged fingerprint drawing can be collected by placing the paper onto our proof-of-concept display. The result indicates the great potential of using our multifunctional display for future on-screen multi-point fingerprint recognition on increasing the display resolution.

In addition, the high brightness of our device at the LED mode and high photosensitivity at the detector mode allow us to use the proof-of concept display to monitor PPG of human bodies, which is of critical importance in medical and health monitoring. We show the PPG signal captured by our proof-of-concept display that uses 10 × 10 pixels as

LEDs and another 10 × 10 pixels in the adjacent area as photodetectors (Supplementary Fig. 12). For comparison, we simultaneously record PPG signals captured by a commercial PPG sensor based on a III-V LED and Si photodetector. We observe similar PPG signals obtained by our display compared to the commercial one, indicating that our display shows a decent signal to noise ratio for monitoring the PPG signals.

Finally, benefiting from the decent light-to-electricity conversion efficiencies of our red-emissive LEDs, we can make use of these devices to provide electricity for themselves. We show the charging curve of a supercapacitor using the devices as solar cells under the solar simulator (AM 1.5 G conditions) in Fig. 4d. We observe continuously increased voltage to roughly 1.7 V after 1,500 s charging of the supercapacitor, indicating a successful charging process. Subsequently, we can drive our devices in the LED mode with the electricity stored in the supercapacitor, where we observe strong red emission from the devices and decreased voltage of the charged supercapacitor (Fig. 4e). The photovoltaic charging function of the display would enhance the stand-by time of consumer electronic products, especially for some low power consumption products, such as smart watches and smart rings.

Conclusions

We have reported a multifunctional display based on photo-responsive PeLEDs. The display can work as a touch screen, ambient light sensor and image sensor (including fingerprint drawing, which indicates promise as a fingerprint sensor). Such integration of different functions could be used to simplify the structure and decrease the cost of display modules, and could allow ultra-thin and light-weight displays to be created. Moreover, the high photoresponsivity of the pixels makes the display screen a potential platform for human–machine interactions. For example, we show that the screens can be used as a scanner, a PPG sensor and to charge a supercapacitor. Our results illustrate the unique advantages of PeLEDs for display applications and offer a promising route for the development of ultra-thin, multifunctional displays.

Methods

Materials

Formamidinium bromide (FABr), formamidinium iodide and 5-AVAI were purchased from Greatcell Solar Materials Ltd. TFB was purchased from American Dye Source Inc. Caesium bromide (CsBr, 99.99%), lead iodide (PbI_2, 99.99%), lead bromide ($PbBr_2$, 99.99%) and lead chloride ($PbCl_2$, 99.99%) were purchased from Alfa Aesar. 4,7,10-trioxa-1,13-tridecanediamin (TTDDA), 2,2′-(ethylenedioxy)diethylamine (EDEA), polyvinyl pyrrolidine (average molecular weight ~55,000), zinc acetate hydrate ($ZnAc_2{\cdot}2H_2O$, 99.99%) and all the solvents used for device fabrication were purchased from Sigma Aldrich.

Red emitting perovskite precursor

Perovskite precursor solution was prepared by mixing PbI_2 (0.125 M), CsBr (0.25 M), formamidinium iodide (0.25 M) in *N*,*N*-dimethylmethanamide (DMF) and stirred at 60 °C for 1 h. Different amounts of 5-AVAI (0–0.038 M) were further introduced as processing additives. We also incorporated a certain amount of $ZnAc_2{\cdot}H_2O$ (0.125 M) to modulate perovskite films growing process[32–35].

Green emitting perovskite precursor

We prepare perovskite precursor solution by mixing 0.4 M $PbBr_2$, 0.06 M CsBr and 0.54 M FABr in DMF, followed by stirring at 60 °C for 2 h. 0.03 M EDEA was further introduced as processing additive.

Blue emitting perovskite precursors

We prepared perovskite precursor solution for blue PeLEDs following one of our previous publications[36]. CsBr:FABr:$PbBr_2$:$PbCl_2$ with a molar ratio of 1.2:0.3:0.475:0.525 were mixed and dissolved in dimethyl sulfoxide. The precursor concentration of Pb^{2+} is fixed at 0.15 M and an extra 0.015 M TTDDA was introduced as processing additive.

Device fabrication

Prepatterned ITO substrates were cleaned with detergent, rinsed with deionized water and dried with air flow, followed by 15 min of ultraviolet-ozone treatment. ZnO nanocrystals were synthesized and dispersed in ethanol following a previous publication[37]. For red and green emitting device fabrication, the ZnO layer was prepared by spin-coating on the cleaned ITO glass at 4,000 rpm before transferring to a nitrogen filled glovebox. The perovskite precursor solutions were coated on top of ZnO layers at 4,000 rpm for 30 s, and then annealed on a hot plate for 10 min at 120 °C for the red emitting device and 80 °C for the green emitting device. After cooling down, a TFB layer (12 mg ml^{-1} in chlorobenzene) was further coated as the hole transport layer at a spin-coating speed of 4,000 rpm. The devices were finished by evaporating MoO_x (7 nm) and Au (50 nm) as electrodes in a thermal evaporator under a chamber pressure of 2×10^{-4} Pa. For the blue emitting device, a poly(triaryl amine) (PTAA) layer was first prepared by spin-coating the solution (2 mg ml^{-1} in toluene) on the cleaned ITO glass, followed by annealing at 100 °C for 10 min. A (2-(9*H*-carbazol-9-yl)ethyl)phosphonic acid layer was then coated on the PTAA layer by spin-coating its solution (6 mg ml^{-1} in acetone), followed by spin-coating a polyvinyl pyrrolidine layer (from 2 mg ml^{-1} solution in isopropanol) to improve the wetting with the perovskite precursor. The $CsPb(Br_{1-x}Cl_x)_3$ perovskite layer was coated by spin-coating the precursor solution at 4,000 rpm for 30 s. The perovskite layer was finally obtained by annealing at 80 °C for 10 min after a vapour assist treating with DMF[36]. The devices were finished by evaporating TPBi (50 nm), LiF (1.5 nm) and Al (100 nm) under a chamber pressure of 2×10^{-4} Pa. The pixel sizes of all individual devices were 7.25 mm^2, and the sizes of the pixels in displays were 0.2 × 0.3 mm^2. All the pixel sizes were defined by the overlap of the ITO and metal electrodes that can be controlled by using patterned ITO class and an evaporation shadow mask for the metal electrode.

Device characterization

The *J*–*V* curves, EQE and luminance of PeLEDs were measured on a home-built LED testing platform, where a spectrometer (QE Pro, Ocean Optics) coupled with an integrating sphere (FOIS-1) and a source meter (Keithley 2400) were used to measure device emission and electric data at different scanning voltages in a glovebox. The PLQE was measured using an integrating sphere and a spectrometer to collect the excitation and photoluminescence spectra, with a 450 nm continuous wave laser used as the excitation, adjusted using a motor-controlled neutral filter. The emission angular distribution was measured using a Si photodiode positioned at a fixed distance to the device; the relative angle was controlled using a motor-controlled rotation stage. The solar cell performance was measured using the source meter (Keithley 2400) under an AM 1.5 G solar simulator or a commercial LED lamp. The irradiance of the LED lamp on the device was calibrated by integrating the spectrum collected by the spectrometer. The light-to-current conversion EQE of the devices were measured using a solar cell spectral response measurement system (QE-R3011, Enli Technology) at 0 V bias. The dark current noise of the devices was measured using a lock-in amplifier (SR830, Stanford Research System) coupled with a low noise preamplifier (SR570, Stanford Research System). TPC curves of the devices were recorded by an oscilloscope with an input impedance of 50 Ω when the devices were excited by a pulse laser (337 nm, pulse width ~3.8 ns).

Multifunctional display demonstration

Passive-matrix LED displays were fabricated based on PeLED arrays with 32 × 32 pixels. The active area of every pixel was 0.2 × 0.3 mm^2. The ITO and Au electrodes were connected to the data output pins of shift registers in the control unit (Supplementary Fig. 13) to determine the electric potential (5 to 0 V) of the electrodes. Data were written to the shift registers by an open-source electronics platform (Arduino UNO), which was connected to a computer through the communication port.

To measure the photovoltage of the pixels, we used switch arrays to select the pixel and used the analogue read pin of the Arduino UNO to read the photovoltage. The touch screen function of the display was realized through monitoring the photovoltage change of the pixels and performing the corresponding response of the display according to the touch position. To perform the imaging function of the display, we made one pixel work at the LED mode as light source and the adjacent pixel as photodetector to sense the light reflected by the surface of the object above the screen. The image of the object surface was obtained by scanning the light and sensing pixels simultaneously and recording the corresponding photocurrent of the photodetectors. The patterns of a heart shape and fingerprint drawing were printed on white paper with black ink. The size of the patterns is about 1.3×1.6 cm^2. PPG was performed by setting a 10×10 pixel area as LED and the adjacent 10×10 pixel area as photodetector. Current of the photodetectors was monitored by an oscilloscope after amplification by the low noise preamplifier. To demonstrate the energy conversion function of the display, we used the PeLEDs to charge a 0.5 F supercapacitor and monitor the voltage change of the supercapacitor using the source meter. After the voltage reached 2.0 V, the devices were powered by the supercapacitor to work as LEDs.

Data availability

The data that support the findings of this study are available from the corresponding author upon reasonable request.

References

1. Booth, L. & Seligson, D. Energy sensing light emitting diode display. European patent, EP1461795B1 (2009).
2. Choo, K., Lee, G. & Han, M. Electroluminescent display device integrated with image sensor. US patent, US20180151656A1 (2018).
3. Oh, N. et al. Double-heterojunction nanorod light-responsive LEDs for display applications. *Science* **355**, 616–619 (2017).
4. Tan, Z. K. et al. Bright light-emitting diodes based on organometal halide perovskite. *Nat. Nanotechnol.* **9**, 687–692 (2014).
5. Sutherland, B. R. & Sargent, E. H. Perovskite photonic sources. *Nat. Photonics* **10**, 295–302 (2016).
6. Quan, L. N. et al. Perovskites for next-generation optical sources. *Chem. l Rev.* **119**, 7444–7477 (2019).
7. Liu, X. K. et al. Metal halide perovskites for light-emitting diodes. *Nat. Mater.* **20**, 10–21 (2021).
8. Swarnkar, A. et al. Quantum dot–induced phase stabilization of α-CsPbI 3 perovskite for high-efficiency photovoltaics. *Science* **354**, 92–95 (2016).
9. Yang, R. et al. Oriented quasi-2D perovskites for high performance optoelectronic devices. *Adv. Mater.* **30**, 1804771 (2018).
10. Jiang, Q. et al. Surface passivation of perovskite film for efficient solar cells. *Nat. Photonics* **13**, 460–466 (2019).
11. Yoo, J. J. et al. An interface stabilized perovskite solar cell with high stabilized efficiency and low voltage loss. *Energy Environ. Sci.* **12**, 2192–2199 (2019).
12. Jeong, M. et al. Stable perovskite solar cells with efficiency exceeding 24.8% and 0.3-V voltage loss. *Science* **369**, 1615–1620 (2020).
13. Wu, S. et al. Modulation of defects and interfaces through alkylammonium interlayer for efficient inverted perovskite solar cells. *Joule* **4**, 1248–1262 (2020).
14. Lu, H. et al. Vapor-assisted deposition of highly efficient, stable black-phase $FAPbI_3$ perovskite solar cells. *Science* **370**, eabb8985 (2020).
15. Yoo, J. J. et al. Efficient perovskite solar cells via improved carrier management. *Nature* **590**, 587–593 (2021).
16. Jeong, J. et al. Pseudo-halide anion engineering for α-$FAPbI_3$ perovskite solar cells. *Nature* **592**, 381–385 (2021).
17. Bao, C. et al. Bidirectional optical signal transmission between two identical devices using perovskite diodes. *Nat. Electron.* **3**, 156–164 (2020).
18. Liu, D. & Kelly, T. L. Perovskite solar cells with a planar heterojunction structure prepared using room-temperature solution processing techniques. *Nat. Photonics* **8**, 133–138 (2014).
19. You, J. et al. Improved air stability of perovskite solar cells via solution-processed metal oxide transport layers. *Nat. Nanotechnol.* **11**, 75–81 (2016).
20. Zhu, Z. et al. Polyfluorene derivatives are high-performance organic hole-transporting materials for inorganic-organic hybrid perovskite solar cells. *Adv. Funct. Mater.* **24**, 7357–7365 (2014).
21. Yan, L. et al. Charge-carrier transport in quasi-2D Ruddlesden–Popper perovskite solar cells. *Adv. Mater.* **34**, 2106822 (2022).
22. Dou, L. et al. Solution-processed hybrid perovskite photodetectors with high detectivity. *Nat. Commun.* **5**, 5404 (2014).
23. Fang, Y. & Huang, J. Resolving weak light of sub-picowatt per square centimeter by hybrid perovskite photodetectors enabled by noise reduction. *Adv. Mater.* **27**, 2804–2810 (2015).
24. Lin, Q., Armin, A., Lyons, D. M., Burn, P. L. & Meredith, P. Low noise, IR-blind organohalide perovskite photodiodes for visible light detection and imaging. *Adv. Mater.* **27**, 2060–2064 (2015).
25. Bao, C. et al. Low-noise and large-linear-dynamic-range photodetectors based on hybrid-perovskite thin-single-crystals. *Adv. Mater.* **29**, 1703209 (2017).
26. Bao, C. et al. High performance and stable all-inorganic metal halide perovskite-based photodetectors for optical communication applications. *Adv. Mater.* **30**, 1803422 (2018).
27. van Breemen, A. J. J. M. et al. A thin and flexible scanner for fingerprints and documents based on metal halide perovskites. *Nat. Electron.* **4**, 818–826 (2021).
28. García De Arquer, F. P., Armin, A., Meredith, P. & Sargent, E. H. Solution-processed semiconductors for next-generation photodetectors. *Nat. Rev. Mater.* **2**, 16100 (2017).
29. Liang, S. et al. A self-powered, sub-nanosecond-response solution-processed hybrid perovskite photodetector for time-resolved photoluminescence-lifetime detection. *Adv. Mater.* **28**, 10794–10800 (2016).
30. Clifford, J. P. et al. Fast, sensitive and spectrally tuneable colloidal-quantum-dot photodetectors. *Nat. Nanotechnol.* **4**, 40–44 (2009).
31. Fuentes-Hernandez, C. et al. Large-area low-noise flexible organic photodiodes for detecting faint visible light. *Science* **370**, 698–701 (2020).
32. Sun, H. et al. Pb-reduced $CsPb_{0.9}Zn_{0.1}I_2Br$ thin films for efficient perovskite solar cells. *Adv. Energy Mater.* **9**, 1900896 (2019).
33. Swarnkar, A., Mir, W. J. & Nag, A. Can B-Site doping or alloying improve thermal- and phase-stability of all-inorganic $CsPbX_3$ (X=Cl, Br, I) perovskites? *ACS Energy Lett.* **3**, 286–289 (2018).
34. Zhang, L. et al. All-inorganic $CsPbI_3$ quantum dot solar cells with efficiency over 16% by defect control. *Adv. Funct. Mater.* **31**, 2005930 (2021).
35. Bi, C. et al. Stable $CsPb_{1-x}Zn_xI_3$ colloidal quantum dots with ultralow density of trap states for high-performance solar cells. *Chem. Mater.* **32**, 6105–6113 (2020).
36. Karlsson, M. et al. Mixed halide perovskites for spectrally stable and high-efficiency blue light-emitting diodes. *Nat. Commun.* **12**, 361 (2021).
37. Yuan, Z. et al. Unveiling the synergistic effect of precursor stoichiometry and interfacial reactions for perovskite light-emitting diodes. *Nat. Commun.* **10**, 2818 (2019).

Acknowledgements
We thank M. Karlson for preparing the bule PeLEDs. This work was supported by the Swedish Government Strategic Research Area in Materials Science on Functional Materials at Linköping University (Faculty grant SFO-Mat-LiU no. 2009-00971). C.B. acknowledges the support from the Excellent Yang Scholar (Overseas) Fund from National Natural Science Foundation of China. Z.Y. acknowledges the support from the European Union's Horizon 2020 research and innovation programme under grant agreement no. 861985 (PEROCUBE) and the innovation programme under Marie Skłodowska-Curie grant (agreement no. 101105627) that funded by the Engineering and Physical Sciences Research Council (UK) (grant no. EP/Y029135/1).

Author contributions
C.B. and F.G. conceived the idea. Z.Y. designed the compositions of perovskite emitters and the device structure, fabricated the perovskite devices and performed the electroluminescence and photovoltaic efficiency characterizations. C.B. performed the electroluminescence speed and photodetection measurements and the application demonstrations. W.N., Z.W., C.B. and T.Y., optimized the blue emitting devices. J.Y. and J.W. supported the PLQE and angular distribution measurements. C.B. drafted the manuscript. C.B., Z.Y. and F.G. revised and refined the manuscript. All authors discussed the results and commented on the paper.

FundingInformation
Open access funding provided by Linköping University.

Competing interests
C.B., Z.Y. and F.G. have filed a patent based on the concept developed in this paper. The other authors declare no competing interests.

Additional information
Supplementary information The online version contains supplementary material available at https://doi.org/10.1038/s41928-024-01151-x.

Correspondence and requests for materials should be addressed to Feng Gao.

Peer review information *Nature Electronics* thanks Azhar Fakharuddin and the other, anonymous, reviewer(s) for their contribution to the peer review of this work.